2014 Spring

“Advanced Physical Metallurgy”

- Bulk Metallic Glasses -

05.20.2014

Eun Soo Park

Office: 33-313
Telephone: 880-7221
Email: espark@snu.ac.kr
Office hours: by appointment

Radial distribution function - definition

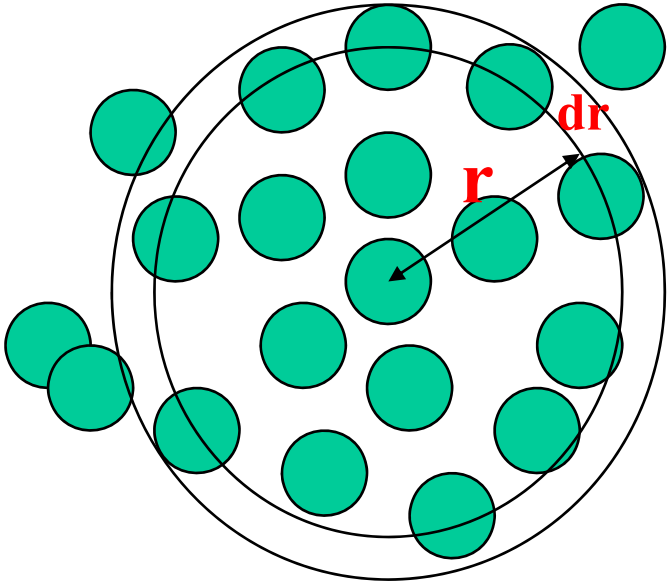

$$g(r) = \frac{1}{\langle \rho \rangle} \frac{dn(r, r+dr)}{dv(r, r+dr)}$$

1. Carve a shell of size r and r + dr around a center of an atom.

   The volume of the shell is

   $dv = 4\pi r^2 dr$

1. Count number of atoms with centers within the shell (dn)
2. Average over all atoms in the system
3. Divide by the average atomic density $\langle \rho \rangle$

Characterizing the structure - radial distribution function,
also called pair distribution function

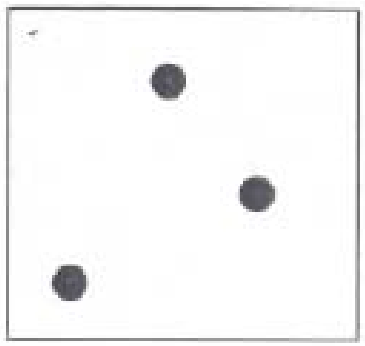

(a)

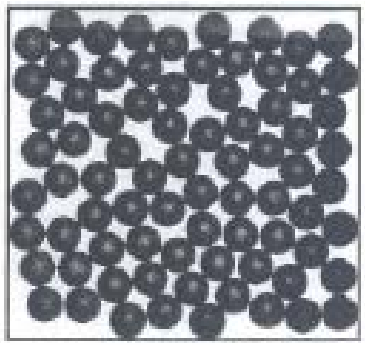

(b)

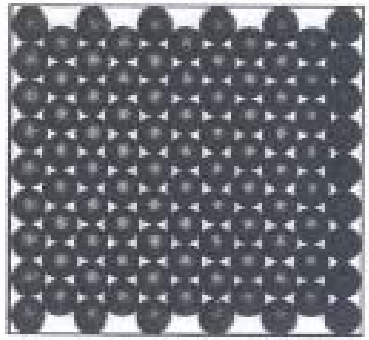

(c)

Figure 2.4 Hard-sphere model of (*a*) gas, (*b*) liquid/glass, and (*c*) crystalline solid.

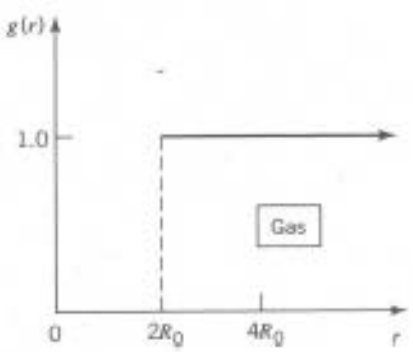

(a)

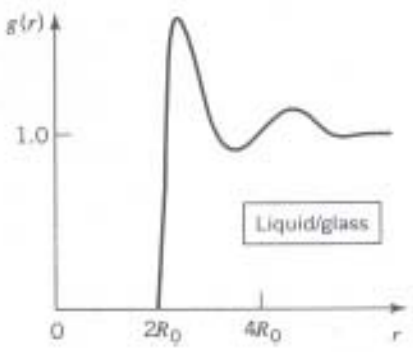

(b)

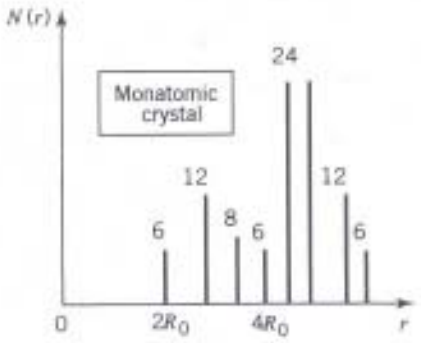

(c)

Figure 2.5 Pair-distribution functions for (*a*) a gas and (*b*) liquid or glass. (*c*) The radial dependence of the number of neighbors $N(r)$ for a primitive cubic crystal with one atom per lattice site.

Gas, amorphous/liquid and crystal structures have very different radial distribution function

Variation of T_g depending on alloy compositions → Broken Bonds

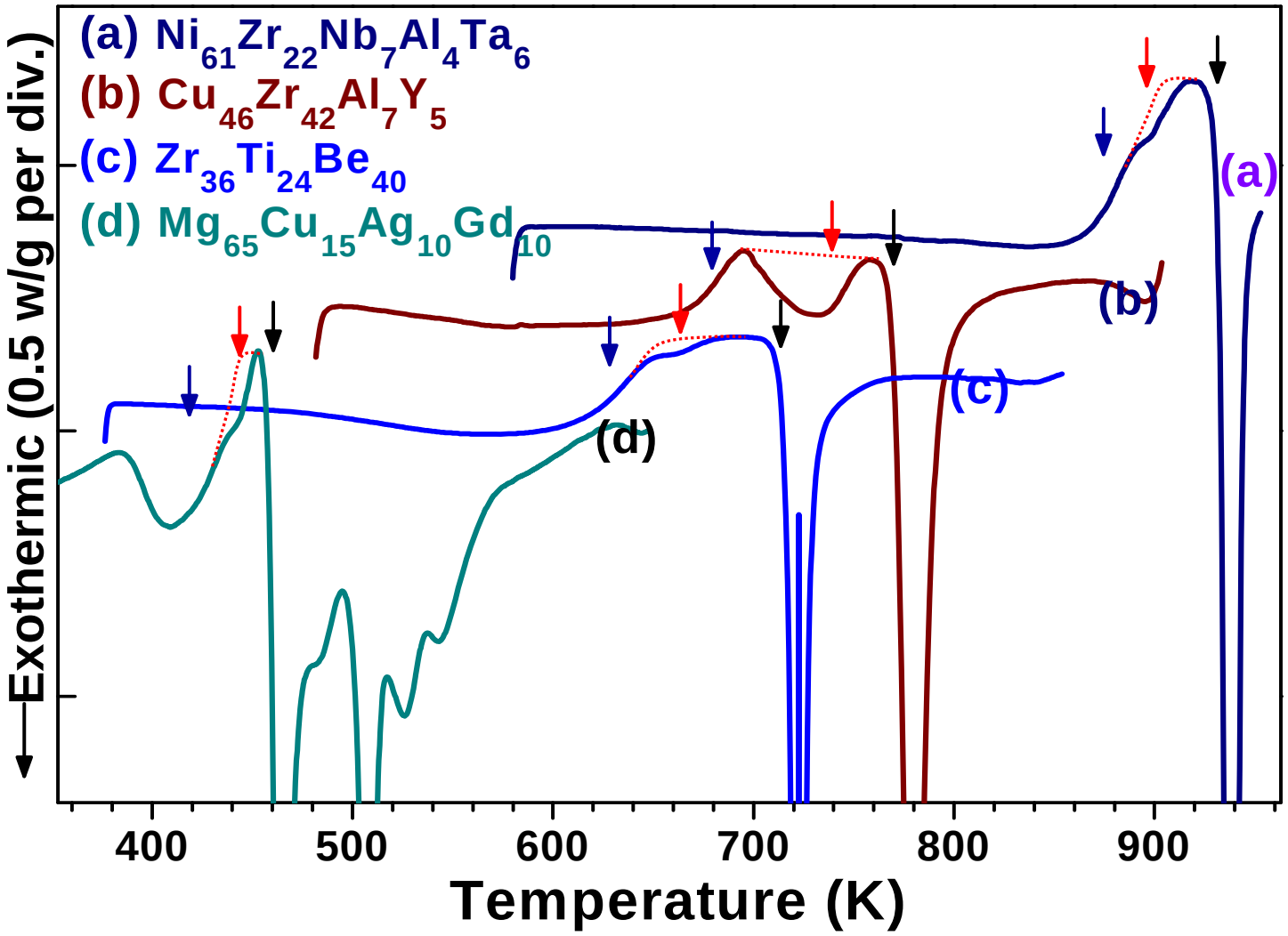

* Typically T_g is ~ 50-60% of the melting point.

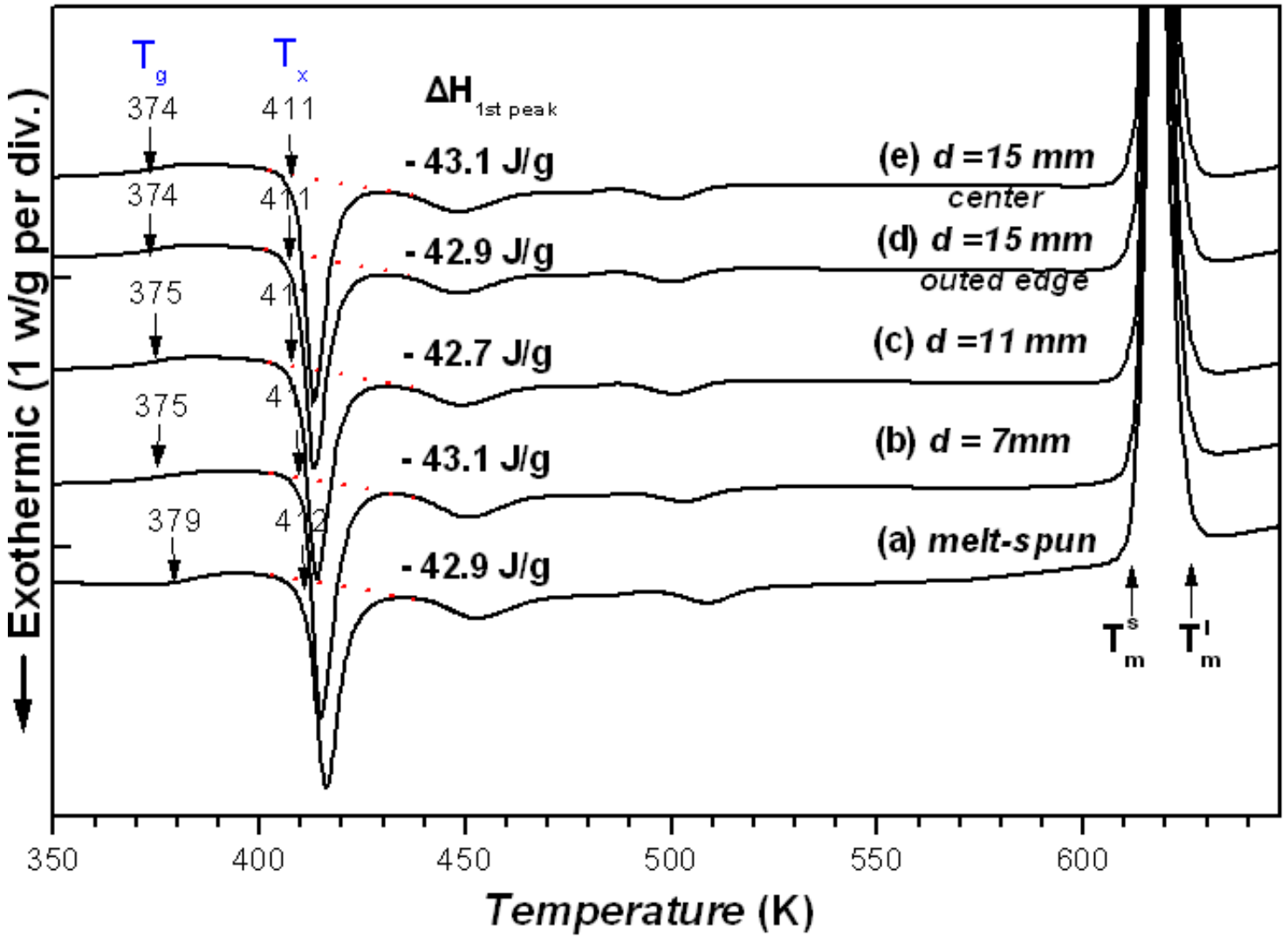

* J Mater Res, 19 (2004) 685.

The glass transition temperature T_g is a kinetic parameter and its value depends on the cooling rate at which the glass is formed (and also on the heating rate at which the glassy sample is reheated). It was also noted that T_g was lower when the glass had formed at lower cooling rates. Therefore, it would be possible to assume that the T_g for the melt-spun ribbon and BMG rod will be different. But, this is not true. The reason is that T_g, the temperature at which the glass is formed is estimated during the cooling of the molten alloy. On the other hand, T_g is usually measured experimentally during the heating of the glassy alloy that has already formed. Once the glass is heated from room temperature to higher temperatures, it is structurally relaxed and, therefore, it does not matter how the glass had initially formed. Accordingly, both types of glasses will have the same T_g and T_x temperatures, when measured at the same heating rate. That is, there is no difference between the T_g values of glasses prepared by RSP or slow solidification methods.

• Amorphous vs Nanocrystalline

2) *Thermal analysis*

Investigation of Glass Structure using DSC

Crystallized volume fraction in glass → Corresponding heat release

a) *glass* → *nucleation & growth*

(perfect random)

J-M-A Eq. $x = 1 - \exp(-bt^n)$ → $-\frac{dH}{dt} = \Delta H(1-x)n \cdot bt^{n-1}$

(***n: 2~4, nucleation mechanism***)

b) *local clustering*: quenched-in nuclei *only growth*

c) *Nanocrystalline* → *growth*

$$\frac{dr}{dt} = M \cdot \frac{\gamma}{r^m} \rightarrow -\frac{dH}{dt} = H(0) \cdot r(0) \cdot M\gamma / r^{m+2}$$

(***M*: atomic mobility, γ : interfacial surface tension**)

(***H(0)*: zerotime enthalpy of a grain size of r (0)**)

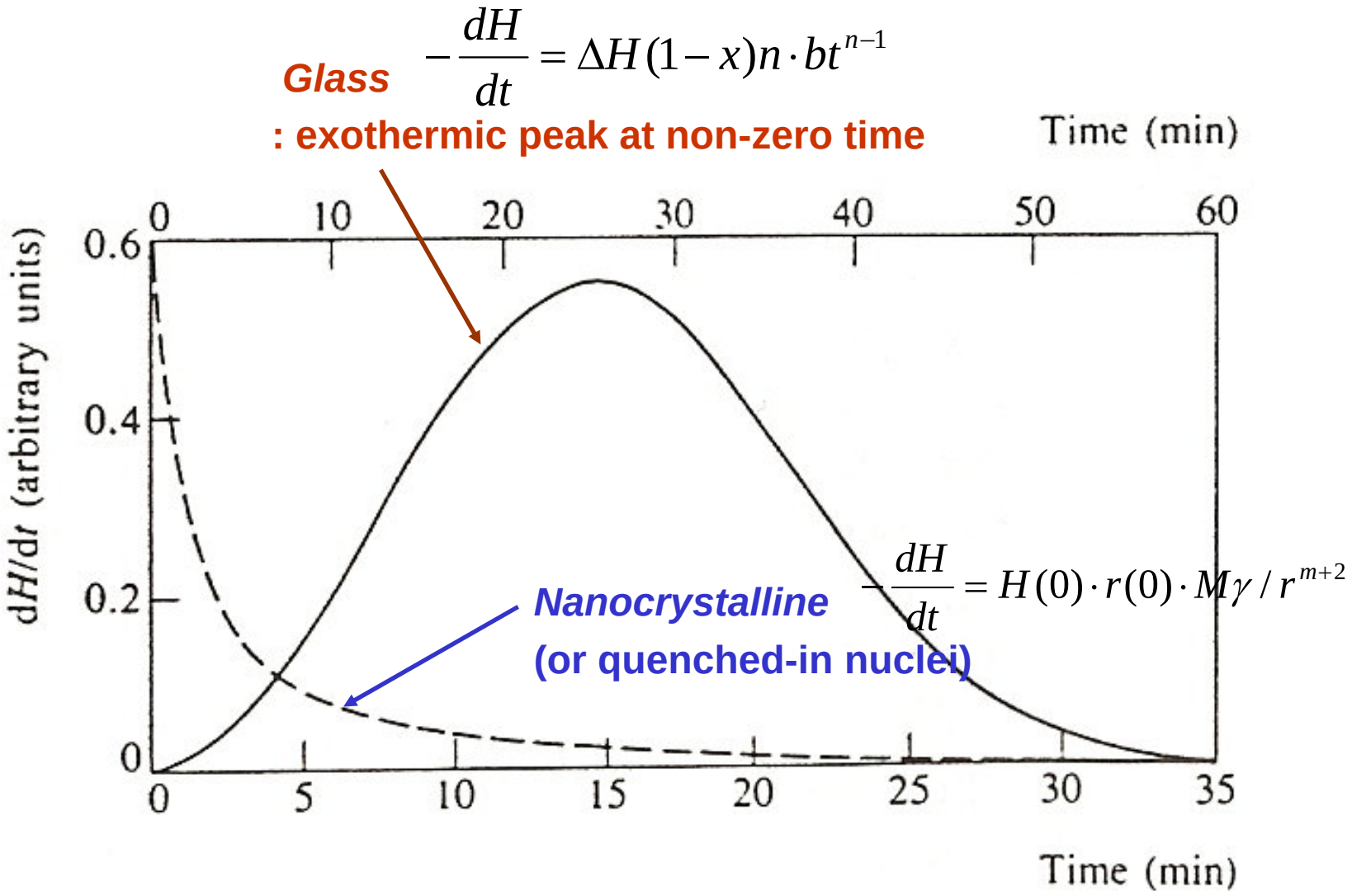

Fig. 1.4 Isothermal enthalpy release rates for crystallite nucleation and growth (solid line) and crystallite grain-coarsening mechanisms (dashed line)

• Amorphous vs Nanocrystalline

1) Microstructural observation

XRD, (HR)TEM, EXAFS …

2) Thermal analysis

DSC (Differential Scanning Calorimetry)

: Measure heat absorbed or liberated during heating or cooling

cf) - glass → nucleation & growth

(perfect random)

- *local clustering*: quenched-in nuclei → *only growth*
- *Nanocrystalline* → *growth*

→ **local clusters with atomic scale are difficult to identify by conventional observation tools of microstructure.**

: *Characterization of structure by pair distribution function*

3) Intensive Structural Analysis: radial distribution function

Effect of quenched-in quasicrystal nuclei

2 mm rod

(a) $Zr_{63}Ti_5Nb_2Cu_{15.8}Ni_{6.3}Al_{7.9}$

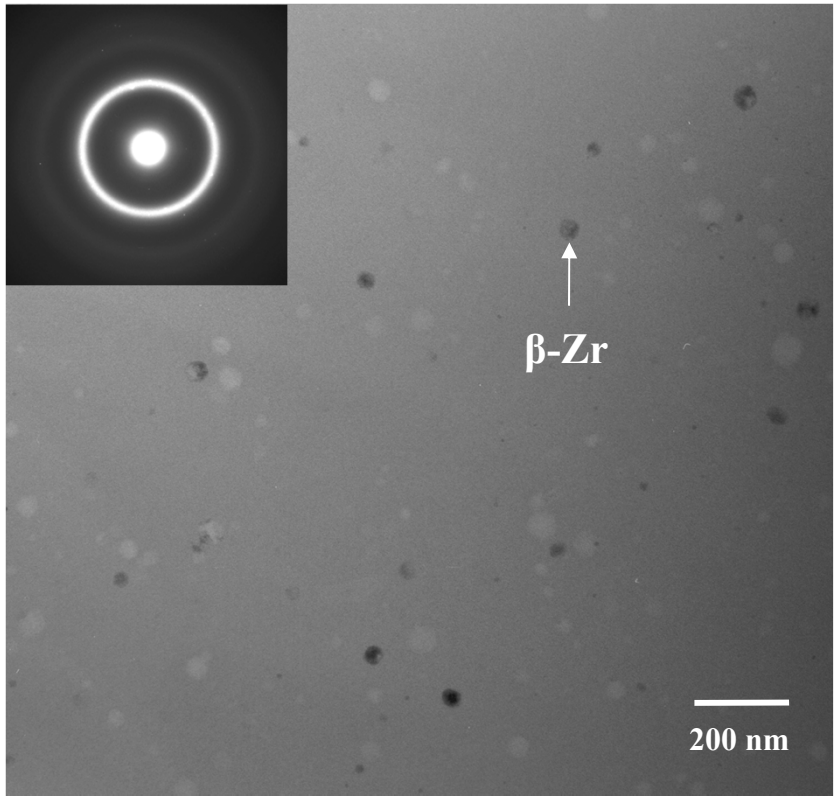

β-Zr particle (~70 nm) in amorphous matrix

(b) $Zr_{57}Ti_8Nb_{2.5}Cu_{13.9}Ni_{11.1}Al_{7.5}$

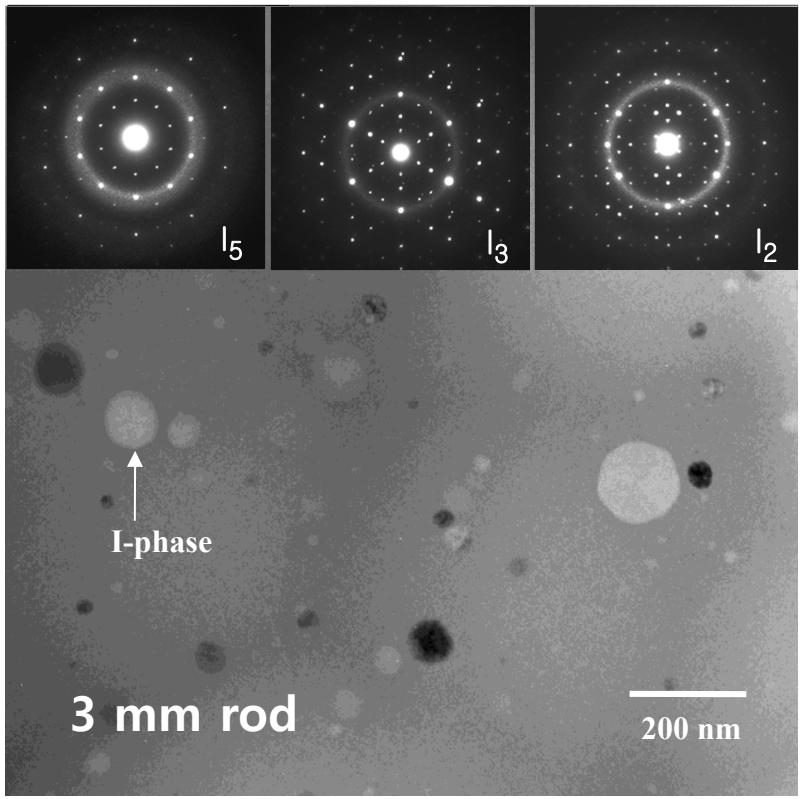

I-phase particle in amorphous matrix

Before deformation

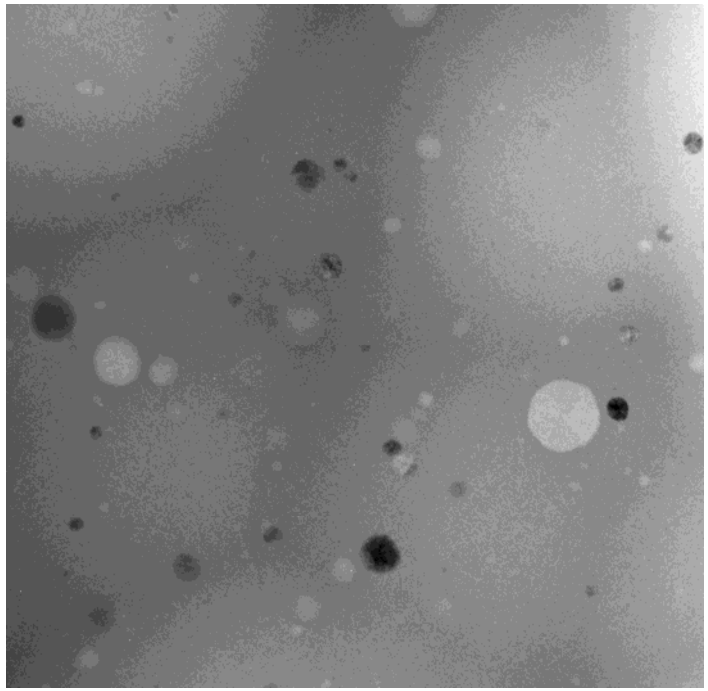

After deformation

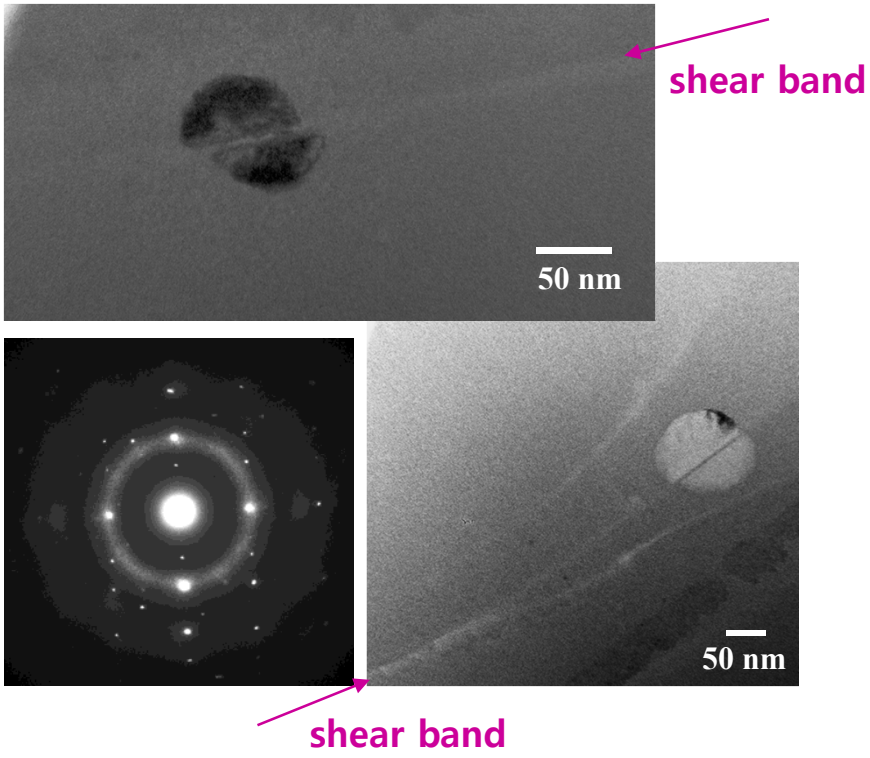

- No distribution of icosahedral particle to blocking the propagation of shear band.
- No enhancement of plasticity in MGMC with icosahedral particle

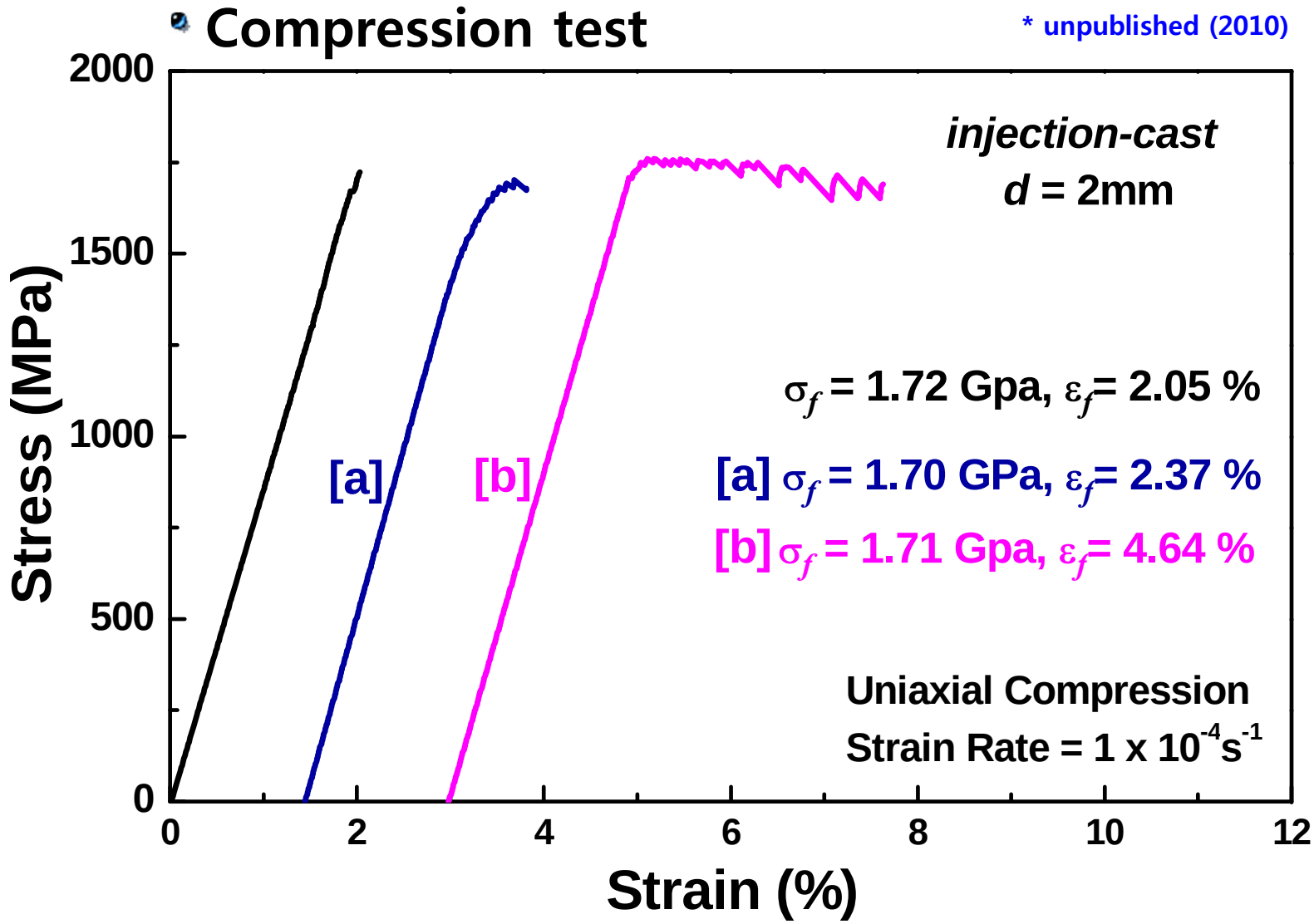
Compression test
* unpublished (2010)
injection-cast
d = 2mm
σf = 1.72 Gpa, εf = 2.05 %
[a] σf = 1.70 GPa, εf = 2.37 %
[b] σf = 1.71 Gpa, εf = 4.64 %
Uniaxial Compression
Strain Rate = 1 x 10-4s-1
[a]
[b]
Stress (MPa)
Strain (%)
0
500
1000
1500
2000
0
2
4
6
8
10
12

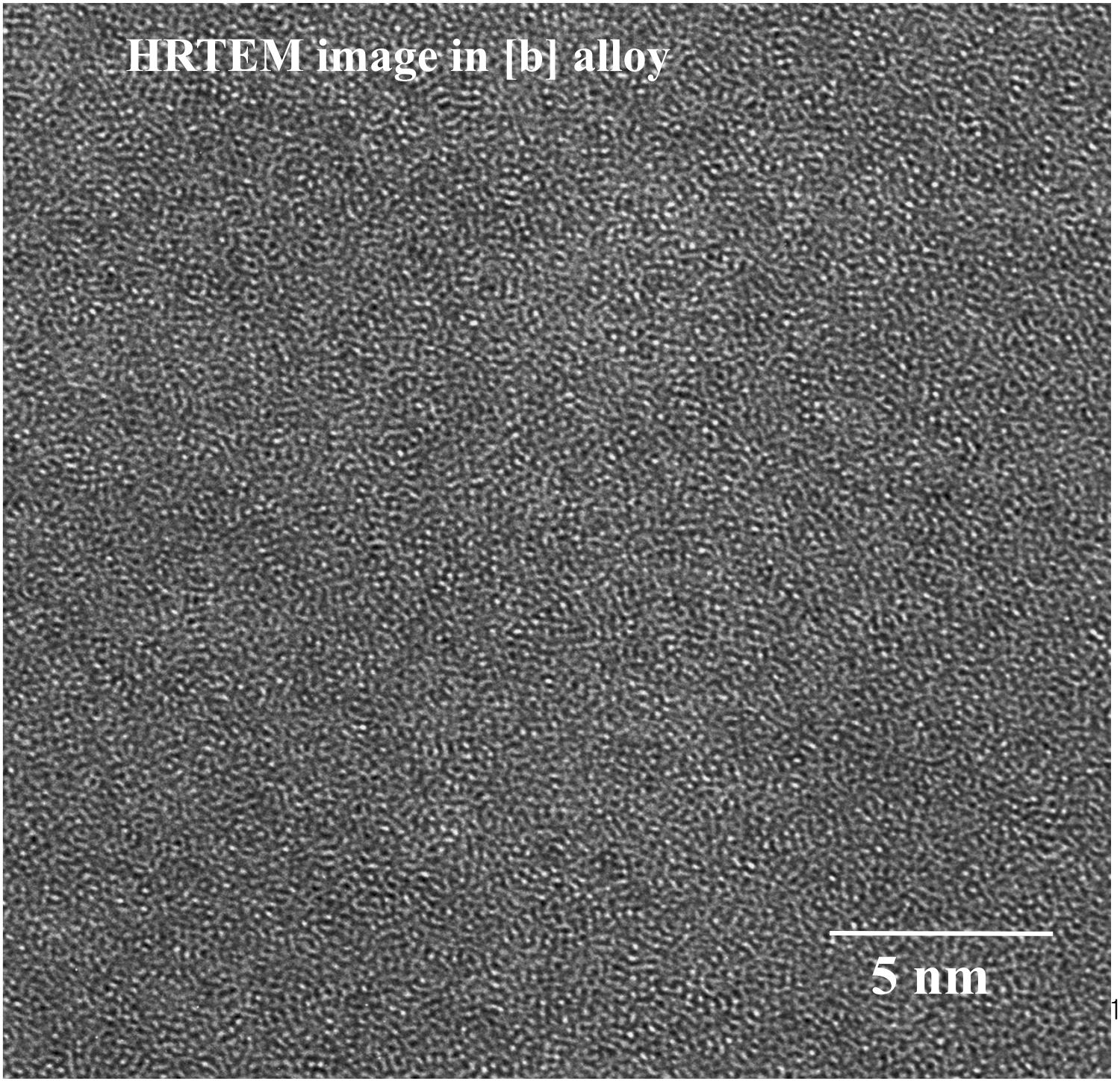
HRTEM image in [b] alloy
5 nm

Activation E : driving force for nucleation

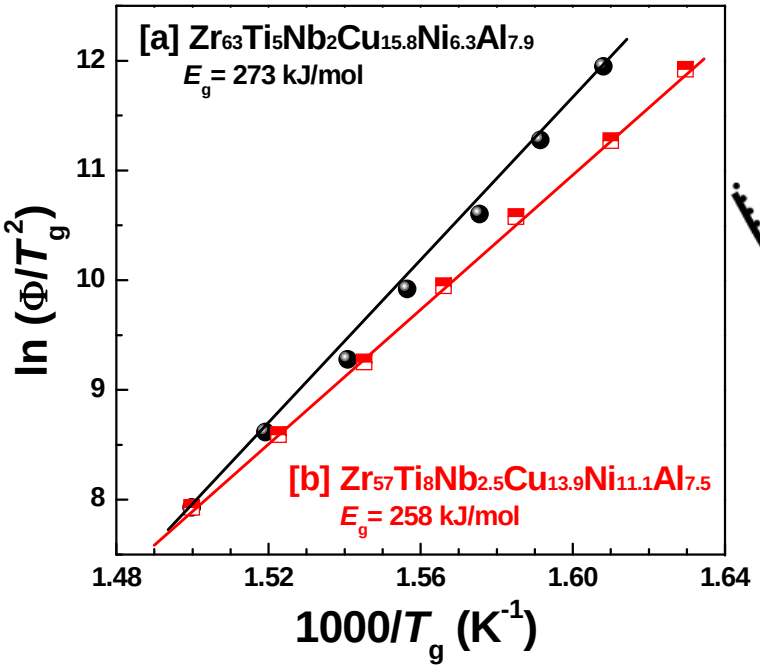

Kissinger's equation

$$\ln(\Phi / T_g^2) = -Q / RT_g + const.$$

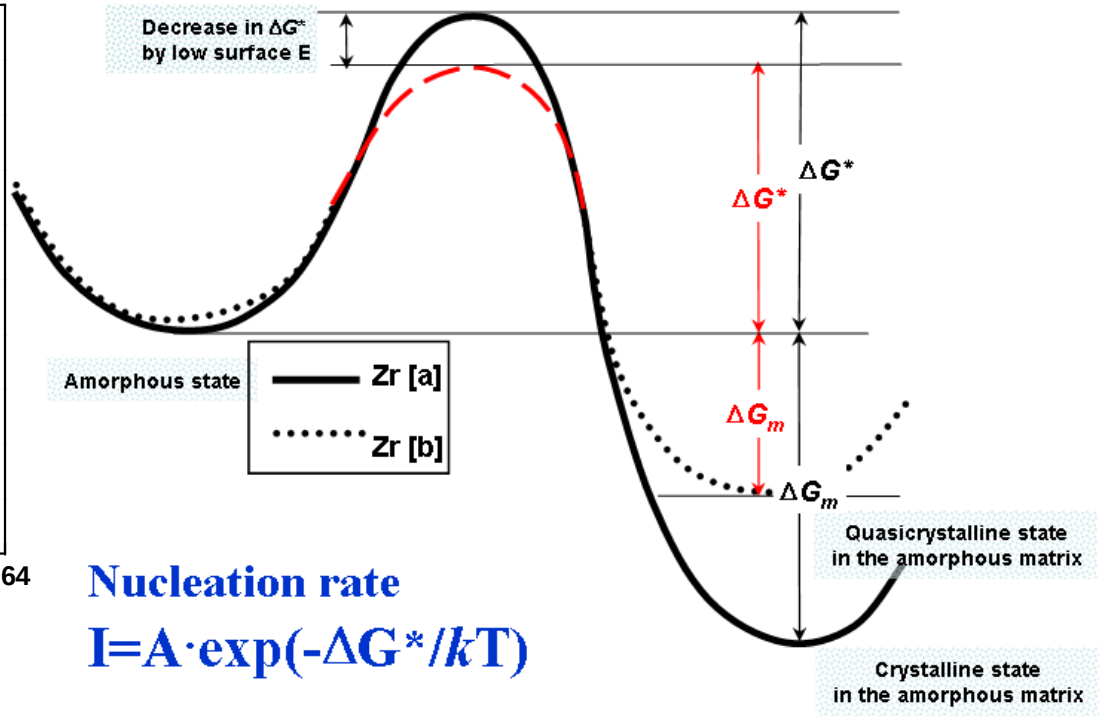

Nucleation rate

$$I = A \cdot \exp(-\Delta G^* / kT)$$

Effect of quenched-in quasicrystal nuclei

- Isotherm in DSC

Isothermal annealing

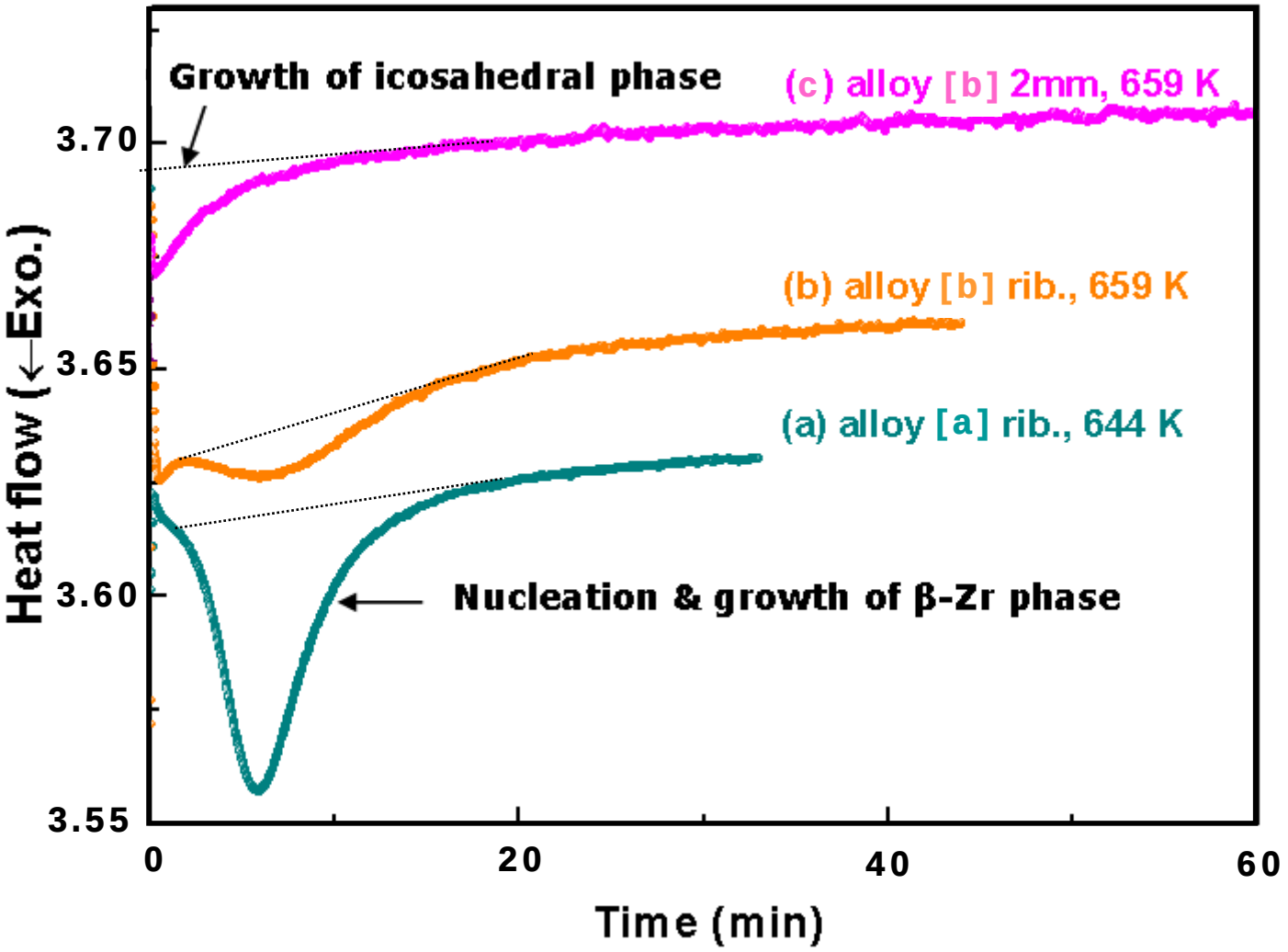

Effect of quenched-in quasicrystal nuclei

- **EXAFS analysis**

(b) $Zr_{57}Ti_8Nb_{2.5}Cu_{13.9}Ni_{11.1}Al_{7.5}$

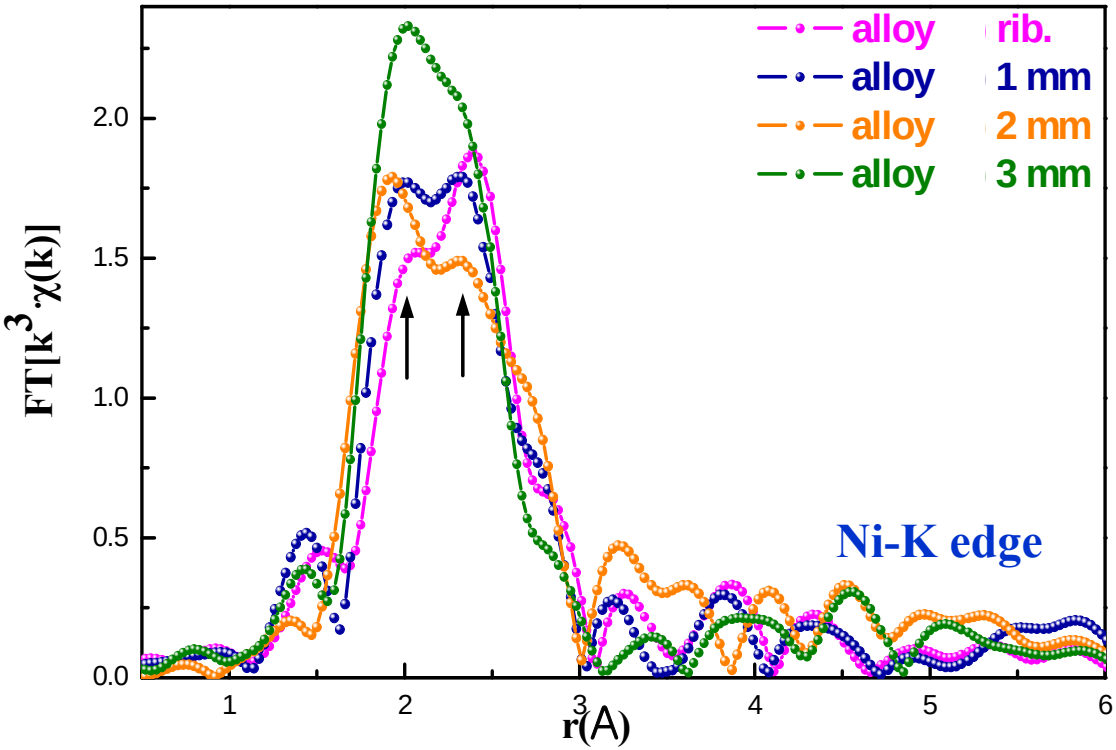

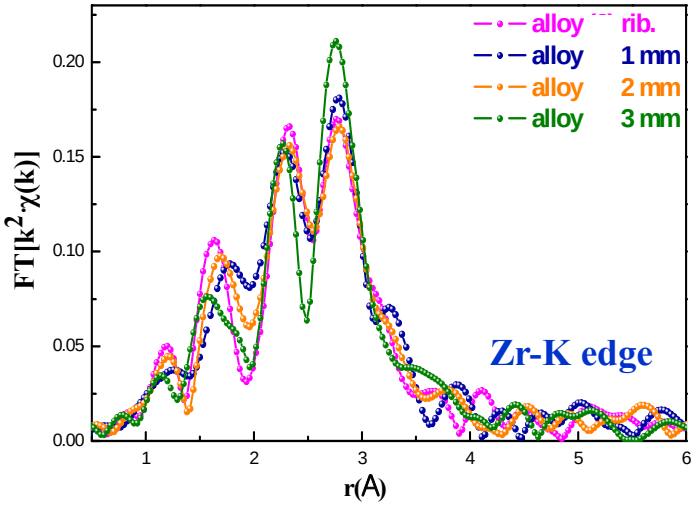

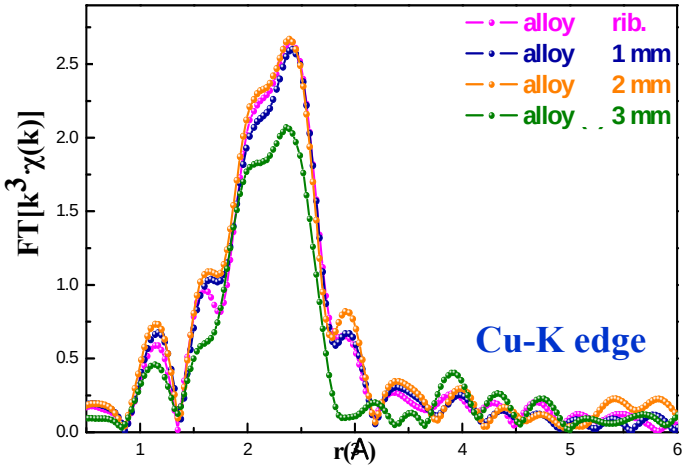

Distinctive structural change around Ni atom

Intensity change due to microstructural change

5.3 Crystallization Modes in Melt-Spun Ribbons

Variables : **solid solubility, number of stable & metastable intermetallic phases, composition**

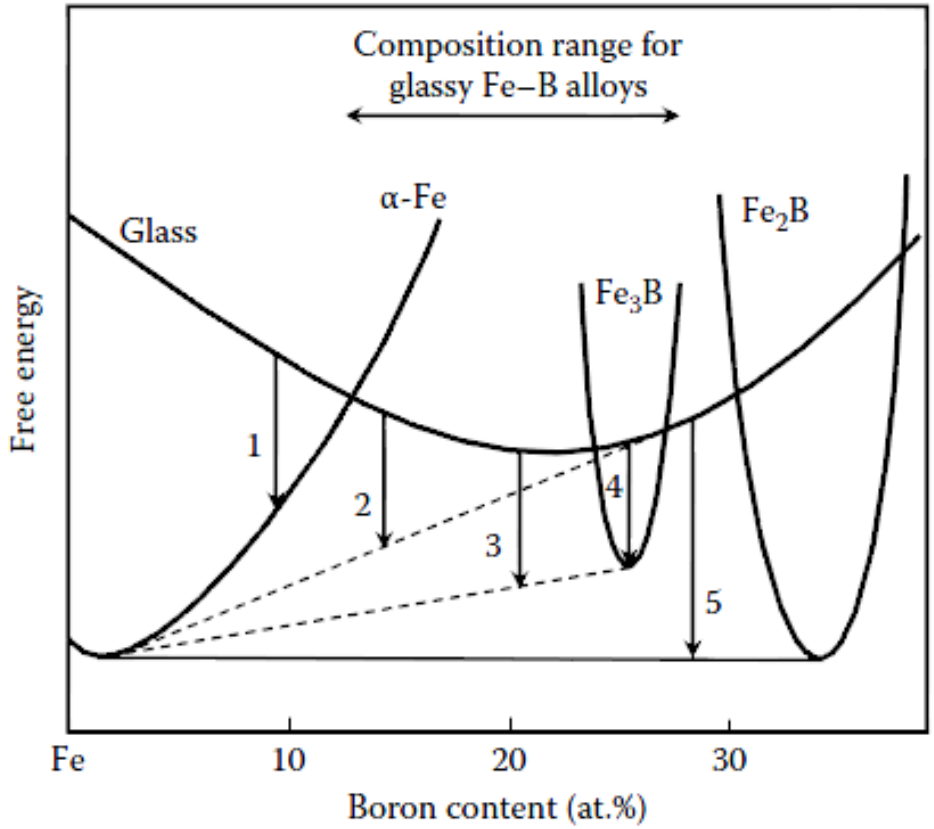

FIGURE 5.5

Hypothetical free energy vs. composition diagram for the Fe-rich Fe–B alloy system. The variation of free energy with composition is represented for the equilibrium α-Fe solid solution and the Fe_2B phases and the metastable Fe_3B phase and the glassy phase. The use of the common tangent approach will help in determining the compositions of the individual phases. The solid common tangent line represents the stable equilibrium between α-Fe and Fe_2B phases, while the dotted common tangent lines represent the metastable equilibrium between α-Fe and Fe_3B phases and α-Fe and glassy phases.

THERMODYNAMICS OF CRYSTALLIZATION

Crystallization Behaviors in Metallic Glass

Metallic glasses crystallize by a nucleation and growth process.

The driving force is the free energy difference between the glass and the appropriate crystalline phase. → (Free energy vs. Composition diagram)

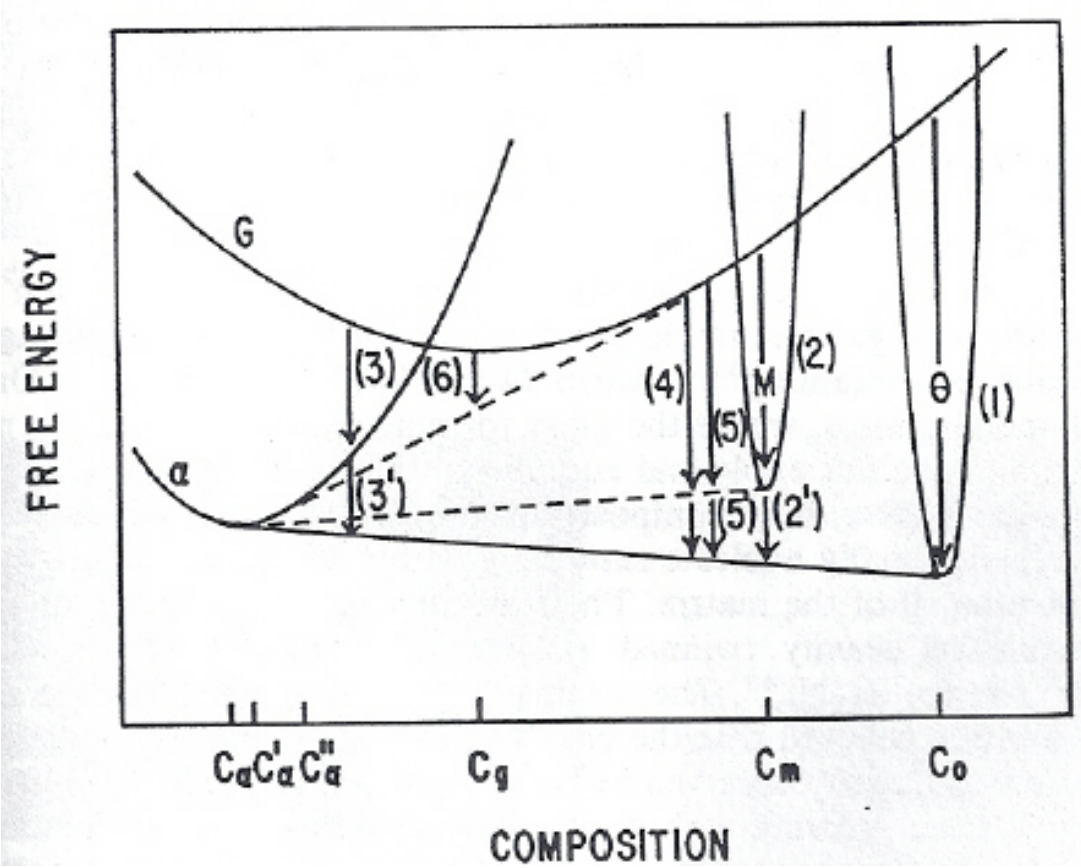

Crystallization mechanisms

1. **Polymorphous Crystallization**
2. **Eutectic Crystallization**
3. **Primary Crystallization**

G: Glass

α : Solid solution (Crystalline phase)

θ : Intermetallic phase

M: metastable phase

THERMODYNAMICS OF CRYSTALLIZATION

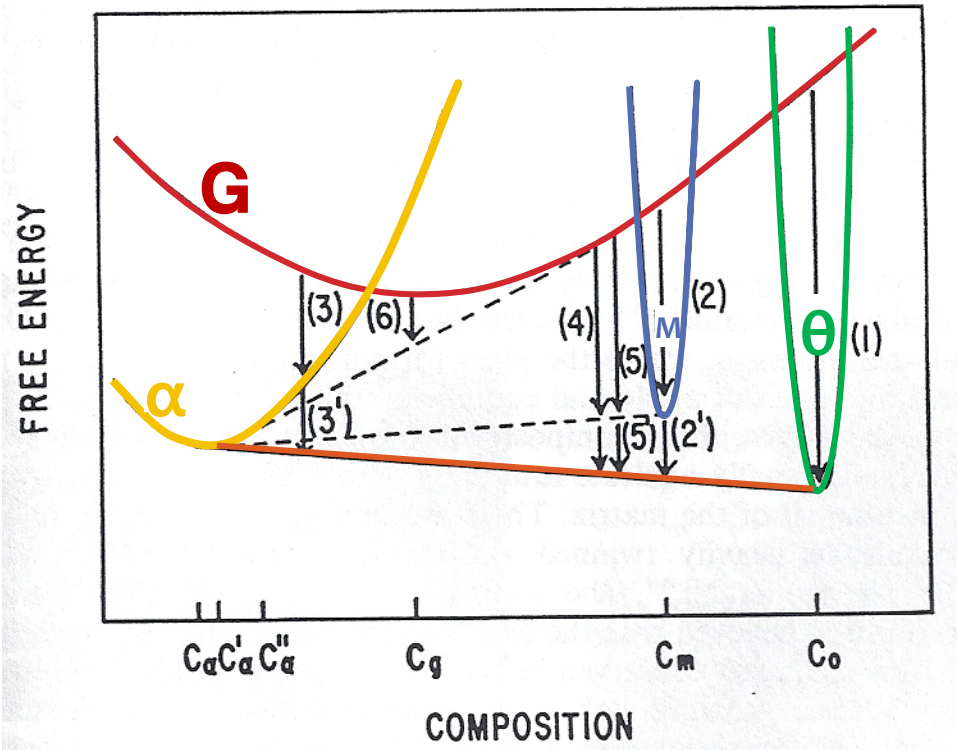

Figure 10.7 Hypothetical free energy diagram to illustrate the crystallization of a metallic glass. G, α, θ, M are respectively the free energy curves of the glass, a terminal solid solution, a stable inter-metallic phase, and a metastable phase. Stable equilibrium is indicated by the solid line; metastable equilibrium by the broken lines. The numbered arrows refer to the devitrification processes described in the text

Crystallization mechanisms

(a) Polymorphous transformation of the glass to a crystalline phase of the same composition.

The product may be either θ (1) or M(2) or a supersaturated solid solution α(3).

In the latter two cases subsequent decomposition can occur to the equilibrium mixture of α and θ (2' and 3')

1. Polymorphous Crystallization: single crystalline phase without any change in composition

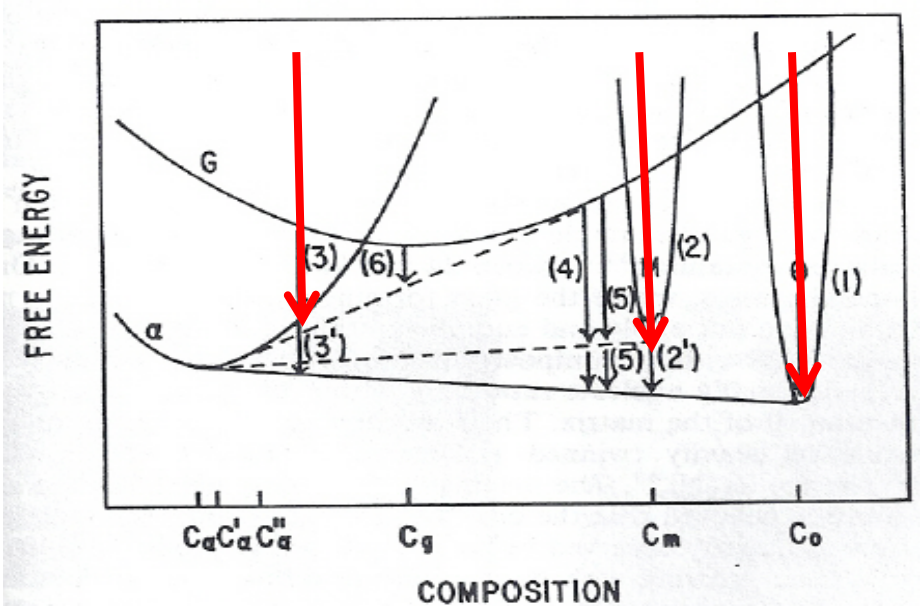

Growth rates and morphologies

$$u = a_0 v_0 \left\{ \exp\left[\frac{-\Delta F_a}{kT} \right] \right\} \left\{ 1 - \exp\left[\frac{-\Delta F_v}{kT} \right] \right\}$$

ΔF_a = activation energy for an atom to leave the matrix and attach itself to the growing phase

ΔF_v = The molar free energy difference btw C and G

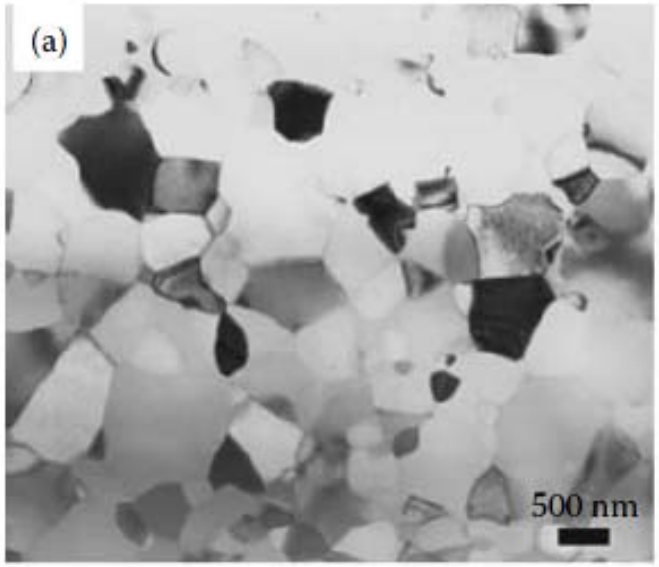

Polymorphous crystallization in a $Ti_{50}Ni_{25}Cu_{25}$ BMG alloy on annealing for 28 min at 709 K.

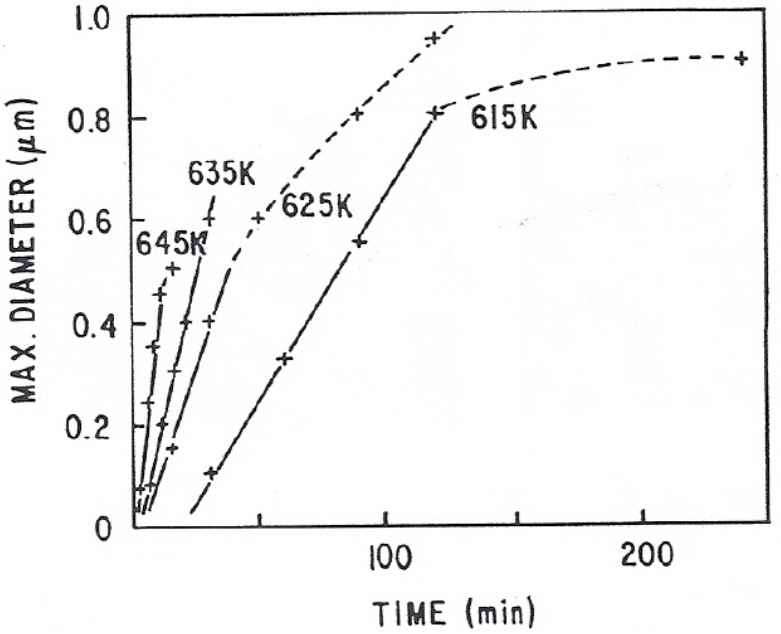

Growth kinetics of Zr_2Ni crystals in glass of same composition The broken lines indicate crystal impingement.

THERMODYNAMICS OF CRYSTALLIZATION

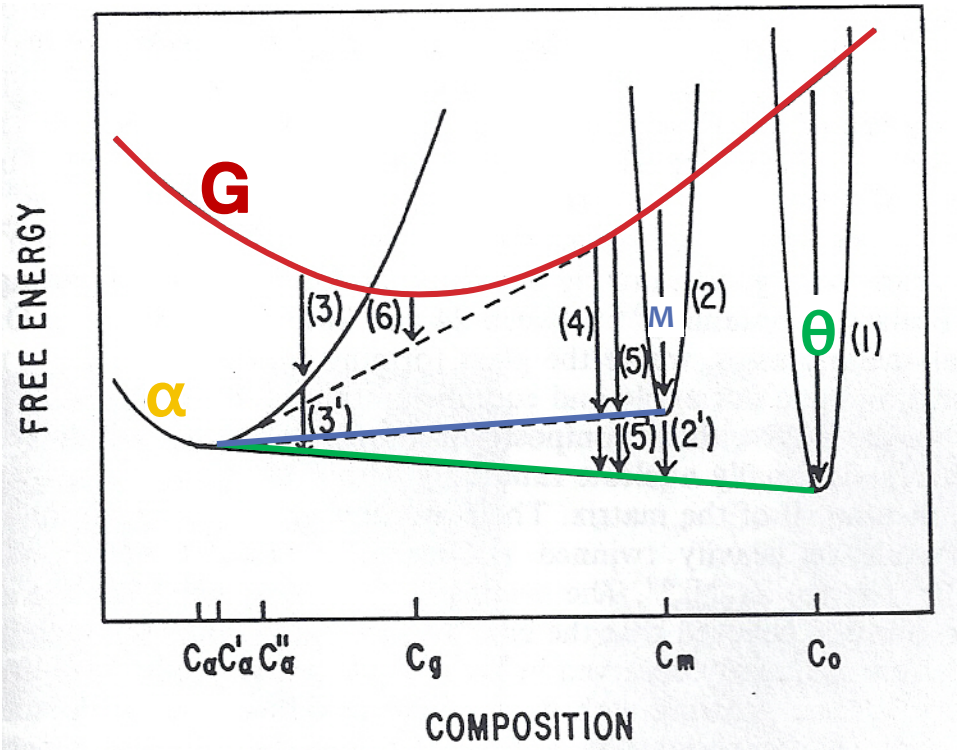

Figure 10.7 Hypothetical free energy diagram to illustrate the crystallization of a metallic glass. G, α, θ, M are respectively the free energy curves of the glass, a terminal solid solution, a stable intermetallic phase, and a metastable phase. Stable equilibrium is indicated by the solid line; metastable equilibrium by the broken lines. The numbered arrows refer to the devitrification processes described in the text

Crystallization mechanisms

(b) Eutectic crystallization of liquids

The glass can reduce its free energy to a point on the common tangent between either α and θ (4) or α and M(5).

In the case of the metastable eutectic between α and M subsequent further decomposition to α and θ can occur. (4' and 5')

2. Eutectic Crystallization

- **Largest driving force**
- **can occur in the whole concentration range between the stable or metastable phases** (Even though the whole transformation takes place in the solid state and therefore it should be more appropriately called a **eutectoid crystallization**, the term "eutectic" has come to stay, presumably because the stating material (the glass) is more liquid-like.)

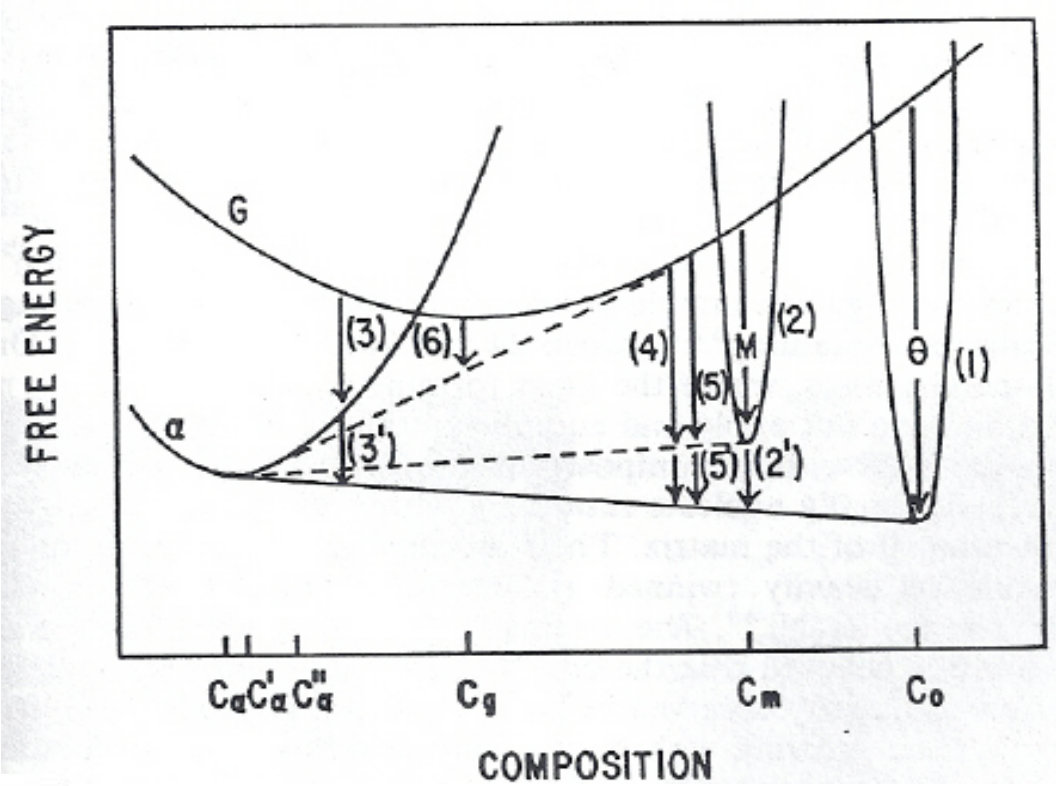

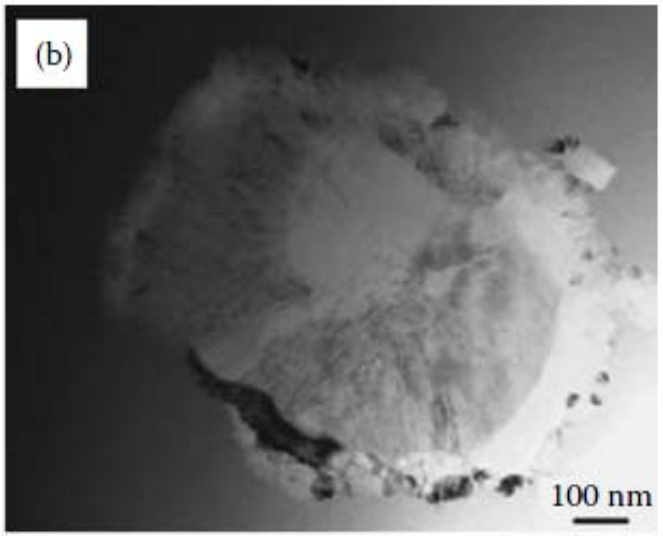

Eutectic crystallization in $Zr_{62.5}Cu_{22.5}Al_{10}Fe_5$ glassy alloy annealed for 10 min. at 713K.

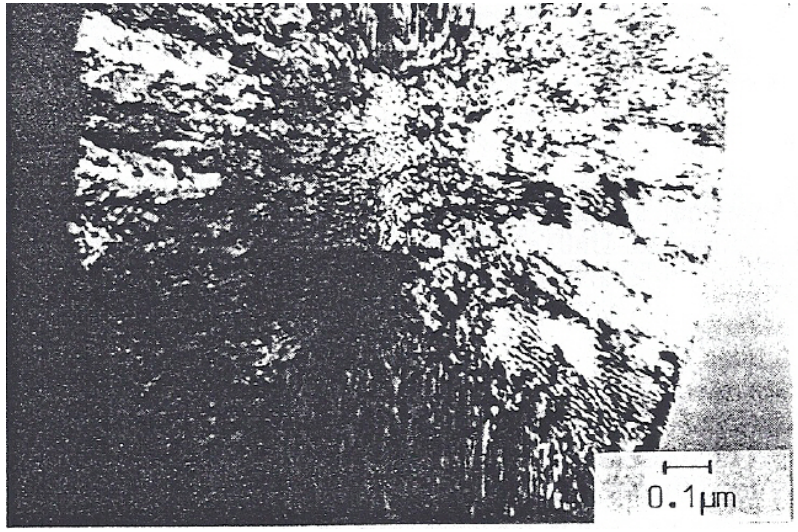

Barrel shaped eutectic crystal in $Fe_{40}Ni_{40}P_{14}B_6$ annealed for 13 min. at 385℃

THERMODYNAMICS OF CRYSTALLIZATION

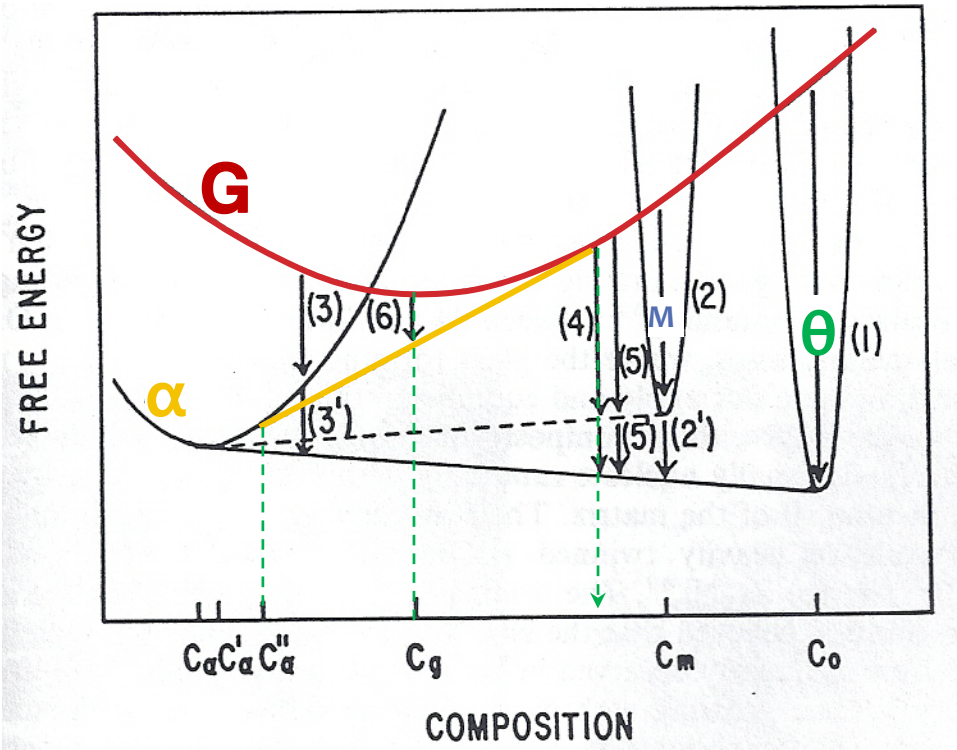

Figure 10.7 Hypothetical free energy diagram to illustrate the crystallization of a metallic glass. G, α, θ, M are respectively the free energy curves of the glass, a terminal solid solution, a stable inter-metallic phase, and a metastable phase. Stable equilibrium is indicated by the solid line; metastable equilibrium by the broken lines. The numbered arrows refer to the devitrification processes described in the text

Crystallization mechanisms

(c) Primary crystallization of supersaturated solid solution (6)

Since the α has a composition c_α" which is less than that of the glass c_g solute is rejected from the growing crystals into the glass (4). Ultimately the untransformed, enriched glass (4) transforms by one of the other mechanisms discussed above.

3. Primary Crystallization

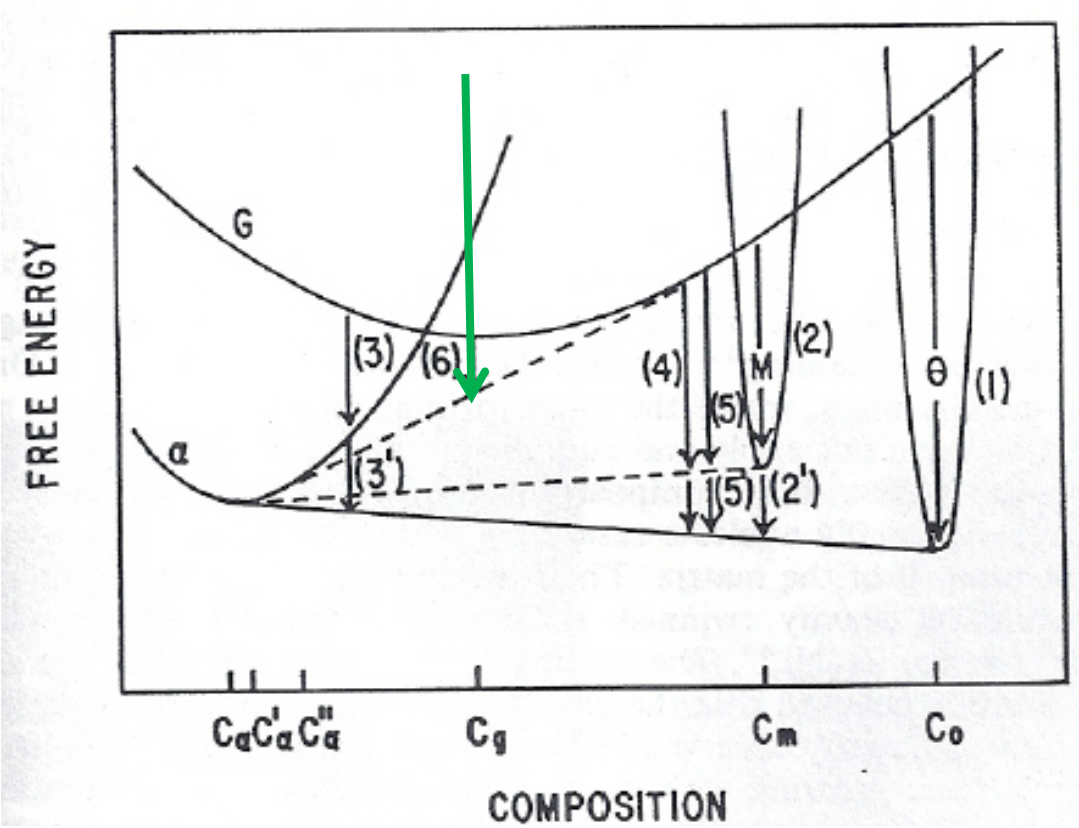

- Forms first from the glass phase
- Supersaturated solid solution
- Since the concentration of the solute in the α-Fe phase is lower than that in the glassy phase, the solute (boron) atoms are rejected into the glassy phase and consequently the remaining glass phase becomes enriched in B until further crystallization is stopped.

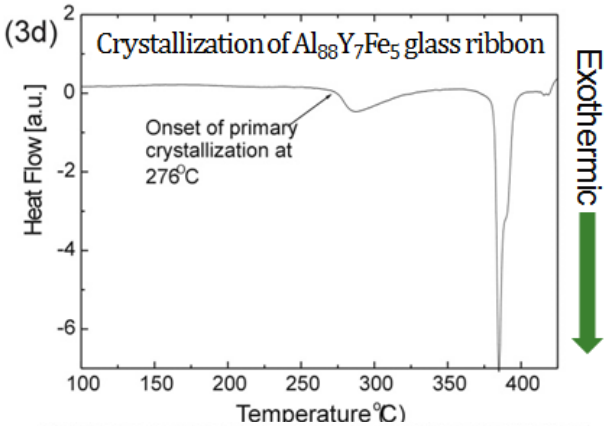

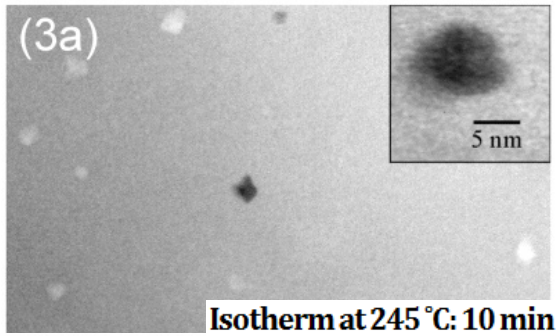

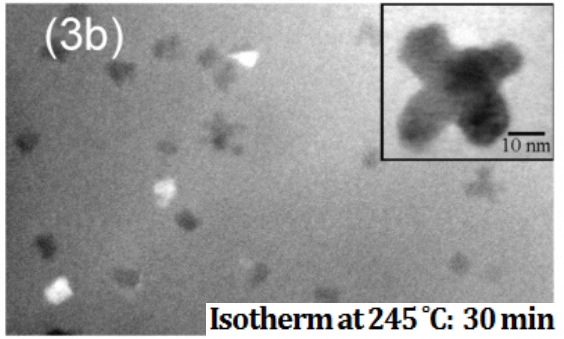

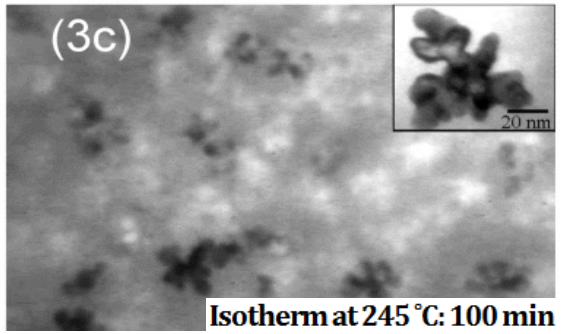

5.5. Thermal Stability of Metallic Glasses

(a) Variation of T_g and T_x in the $Zr_{65}Al_xCu_{35-x}$ (x=0, 7.5, 20) alloys

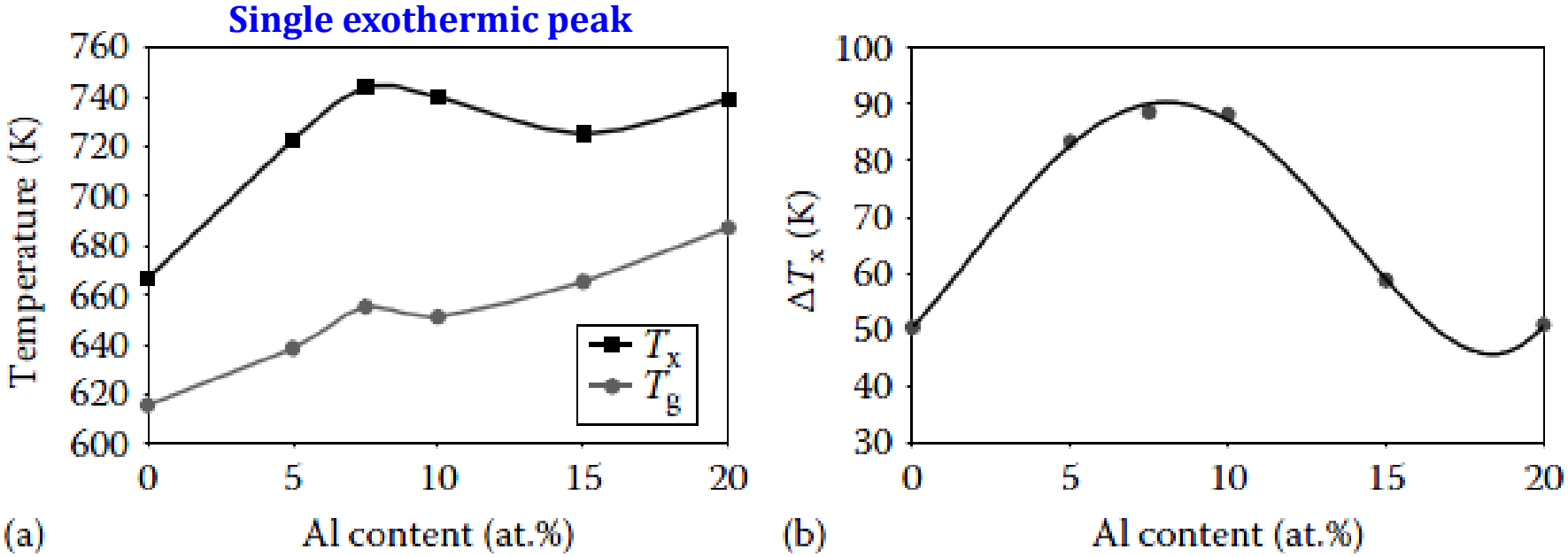

FIGURE 5.7
Variation of (a) T_g and T_x temperatures, and (b) the width of the supercooled liquid region ΔT_x (= $T_x - T_g$), with Al content in the $Zr_{65}Al_xCu_{35-x}$ glassy alloys. (Reprinted from Inoue, A. et al., *Mater. Sci. Eng. A*, 178, 255, 1994. With permission.)

5.5. Thermal Stability of Metallic Glasses

(b) Arrhenius plot of the incubation time for the precipitation of crystalline phases (τ) in the $Zr_{65}Al_xCu_{35-x}$ (x=0, 7.5, 20) alloys

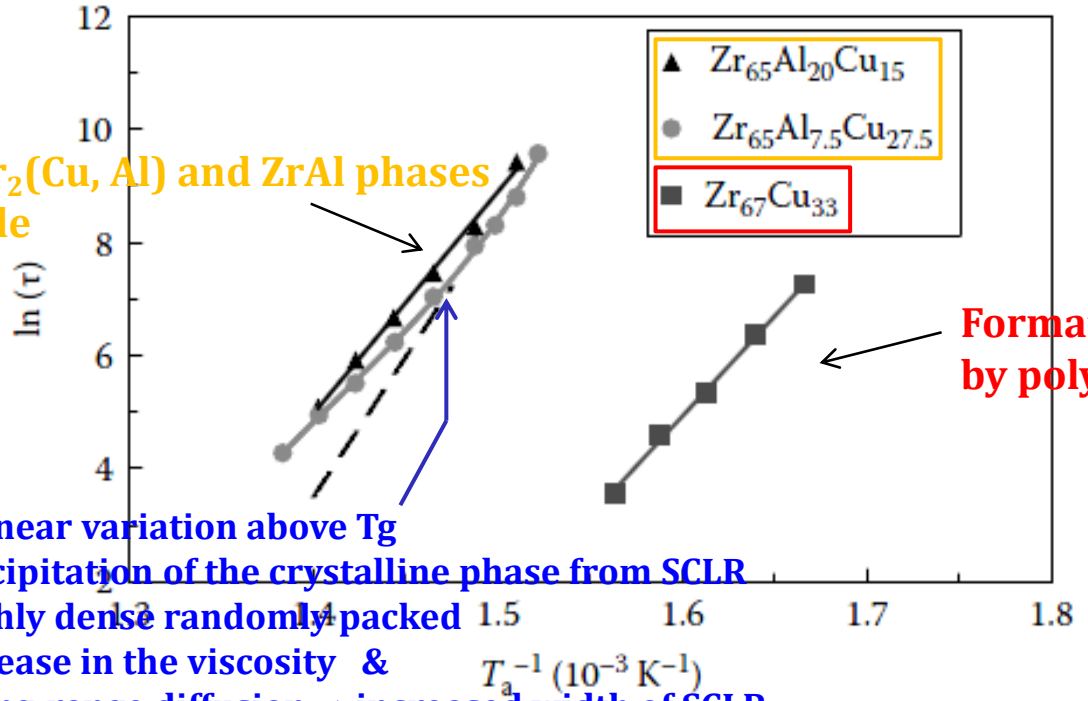

$$\tau \propto \frac{T\eta}{(T_\ell - T)^2}$$

Formation of Zr_2(Cu, Al) and ZrAl phases by eutectic mode

Formation of Zr_2Cu phase by polymorphous mode

Shifted from the linear variation above Tg → suppressed precipitation of the crystalline phase from SCLR due to possess highly dense randomly packed structures → increase in the viscosity & difficult to have long-range diffusion → increased width of SCLR

FIGURE 5.8
Arrhenius plot of the incubation time, τ for the precipitation of crystalline phases in the binary $Zr_{67}Cu_{33}$, and ternary $Zr_{65}Al_{7.5}Cu_{27.5}$ and $Zr_{65}Al_{20}Cu_{15}$ alloys. Note the deviation of τ to the positive side of the linear variation (to higher temperatures) only for the ternary $Zr_{65}Al_{7.5}Cu_{27.5}$ alloy, signifying the delayed crystallization in the alloy with 7.5 at.% Al. Such a deviation is not observed for the other alloys. (Reprinted from Inoue, A. et al., *Mater. Sci. Eng. A*, 178, 255, 1994. With permission.)

(C) Annealing up to T_a at a heating rate of 0.17 K/s (10K/min), annealed there for 60s
→ measure peak temperatures for the nucleation and growth reactions of the crystalline phases in the $Zr_{65}Al_xCu_{35-x}$ (x=0, 7.5) alloys

* Difference in the reciprocals of the Tp between the Pre-annealed and as-quenched samples

688 K, correspond to the peak temp. of the nucleation event of a crystalline phase formation

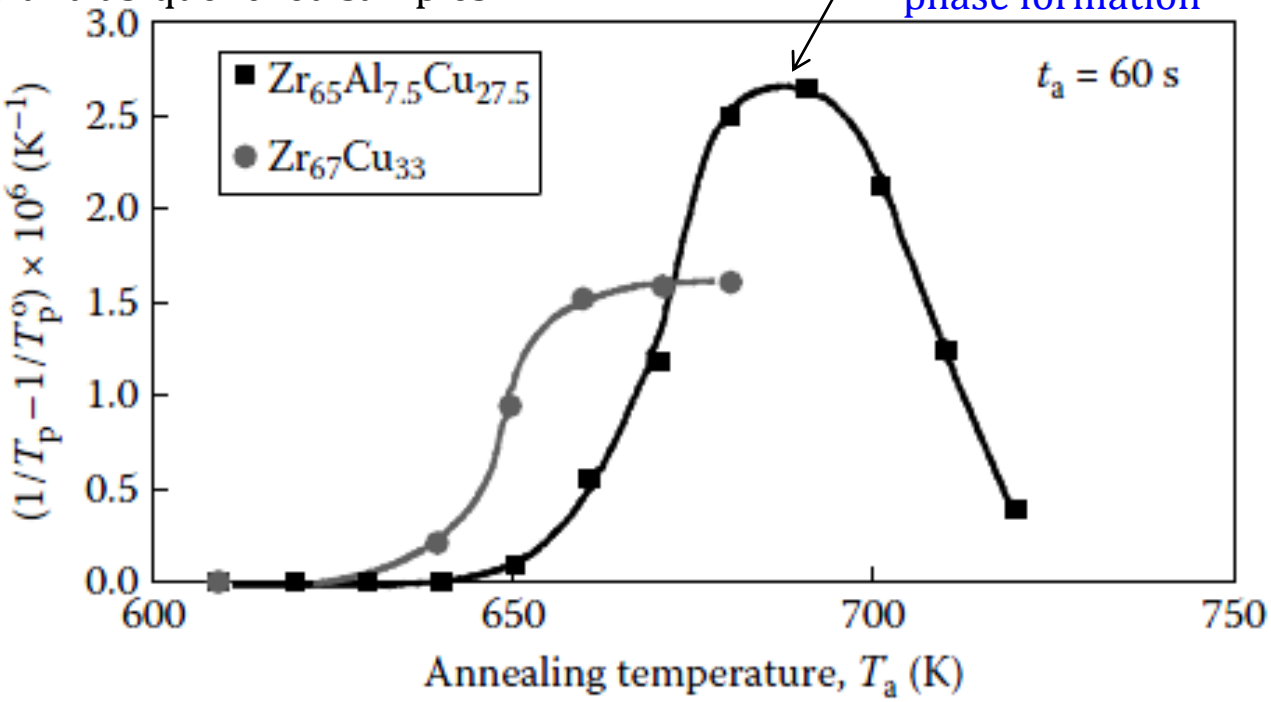

* Measure Tx at a very high heating rate of 5.33 K/s (320 K/min) = corresponding to the maximum growth rates, that is growth temperature
- Zr67Cu33: Just above the maximum temp of 670 K/ difference ~ very small
- Zr65Al7.5Cu27.5: the difference btw max nucleation and max growth temp. ~143K, resulting in enhanced resistance to crystallization (high thermal stability)

* Heating rate ↑ – not significantly increase the grain size in Zr67Cu33 ↔ considerably large grain size in Zr65Al7.5Cu27.5 due to the presence of fewer nuclei

5.6. Crystallization Temperatures and Their Compositional Dependence

Compositional dependence.

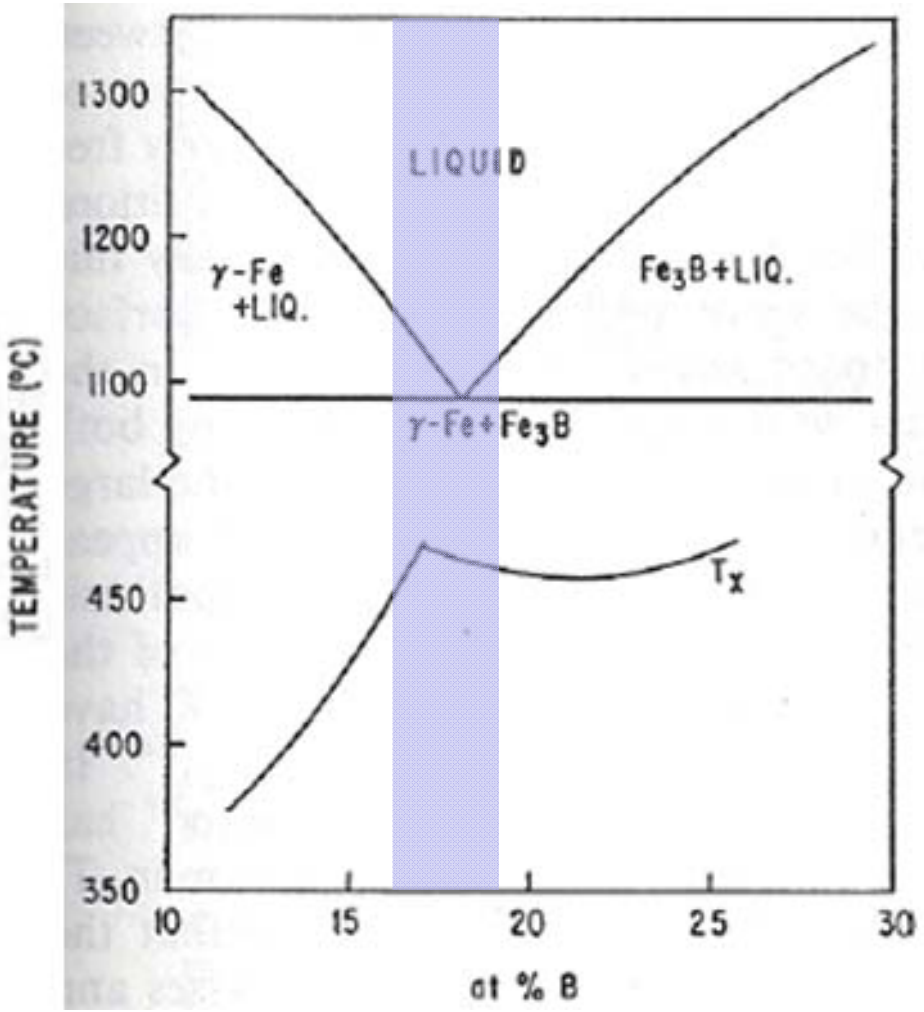

In many binary

Metal-Metalloid glass (Fe-B)

Tx is a maximum near the eutectic composition

The same does not appear to be the case in all-metal glasses

Metal-Metal glass (Ni-Zr)

A monotonic decrease of Tx with increasing Zr content despite the existence in two eutectics

5.6. Crystallization Temperatures and Their Compositional Dependence

Compositional dependence.

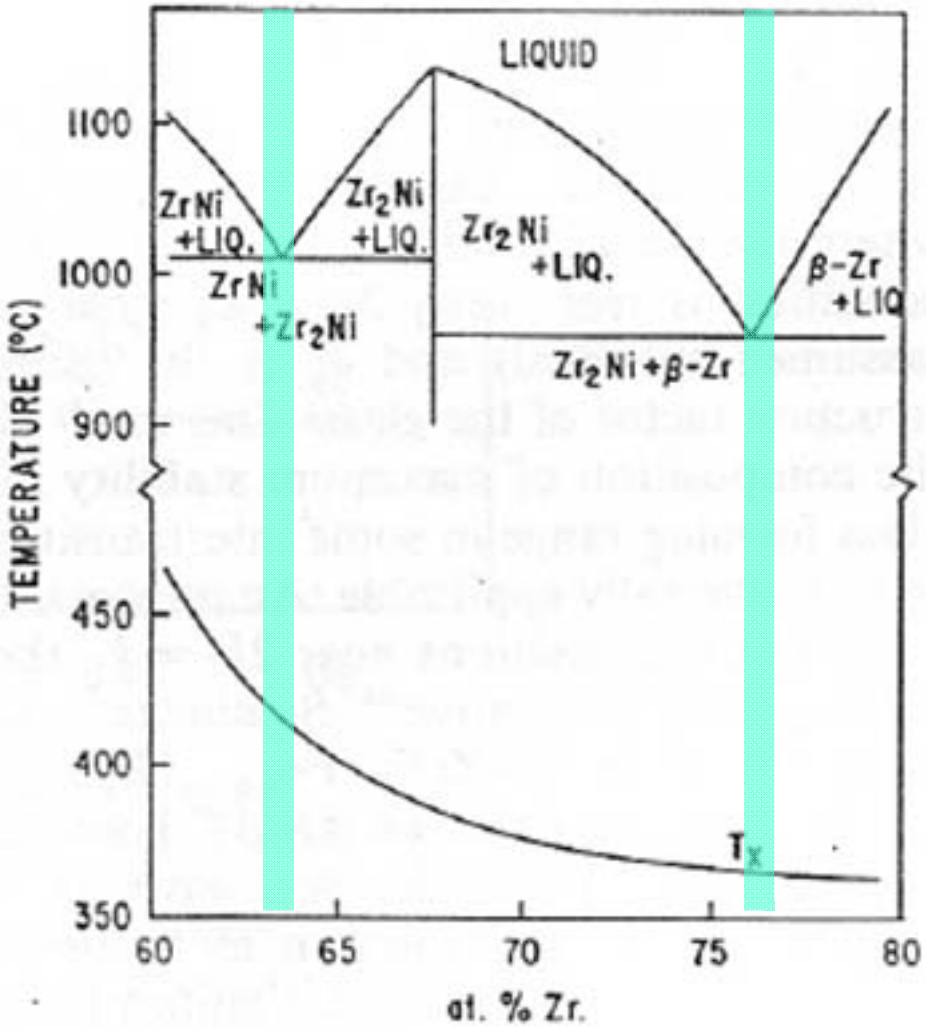

In many binary

Metal-Metalloid glass (Fe-B)

Tx is a maximum near the eutectic composition

The same does not appear to be the case in all-metal glasses

Metal-Metal glass (Ni-Zr)

A monotonic decrease of Tx with increasing Zr content despite the existence in two eutectics

* The degrease in the ΔTx values for the above alloy systems can be attributed to a significant decrease in Tx rather than a slight increase in the Tg value.

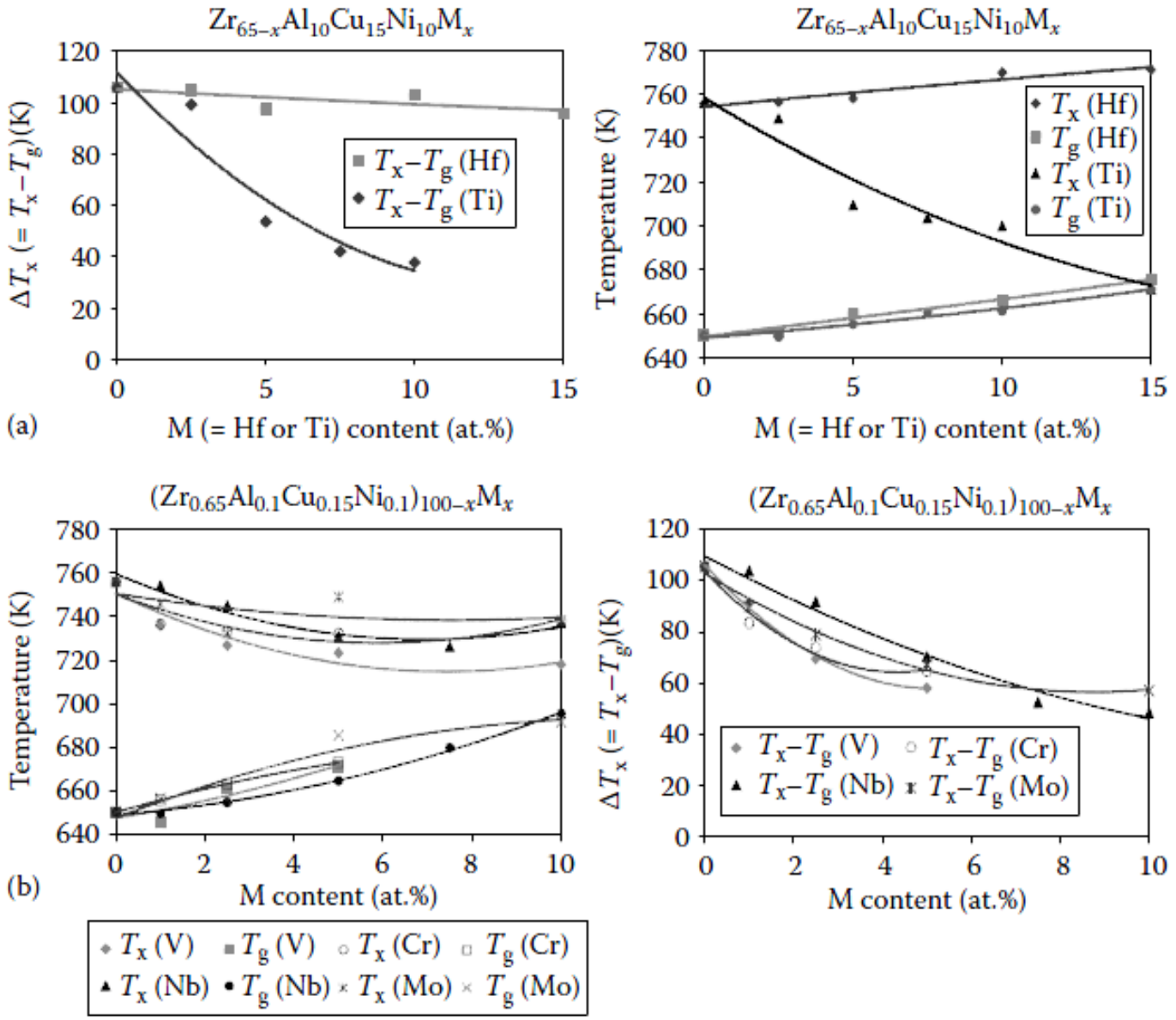

FIGURE 5.10
Variation of T_g, T_x, and ΔT_x with M content for melt-spun glassy alloys of the four groups. (a) $Zr_{65-x}Al_{10}Cu_{15}Ni_{10}M_x$ (where M = Ti and Hf), (b) $(Zr_{0.65}Al_{0.1}Cu_{0.15}Ni_{0.1})_{100-x}M_x$ (where M = V, Nb, Cr, and Mo),

* V. Nb, Cr, Mo, Fe, and Co

→ Highly repulsive to Cu atom

* Pd and Ag with Cu, and

  Ti and Hf with Zr

→ weakly repulsive

: difficult to form densely packed random structure with increasing amount of alloying elements → ΔTx ↓

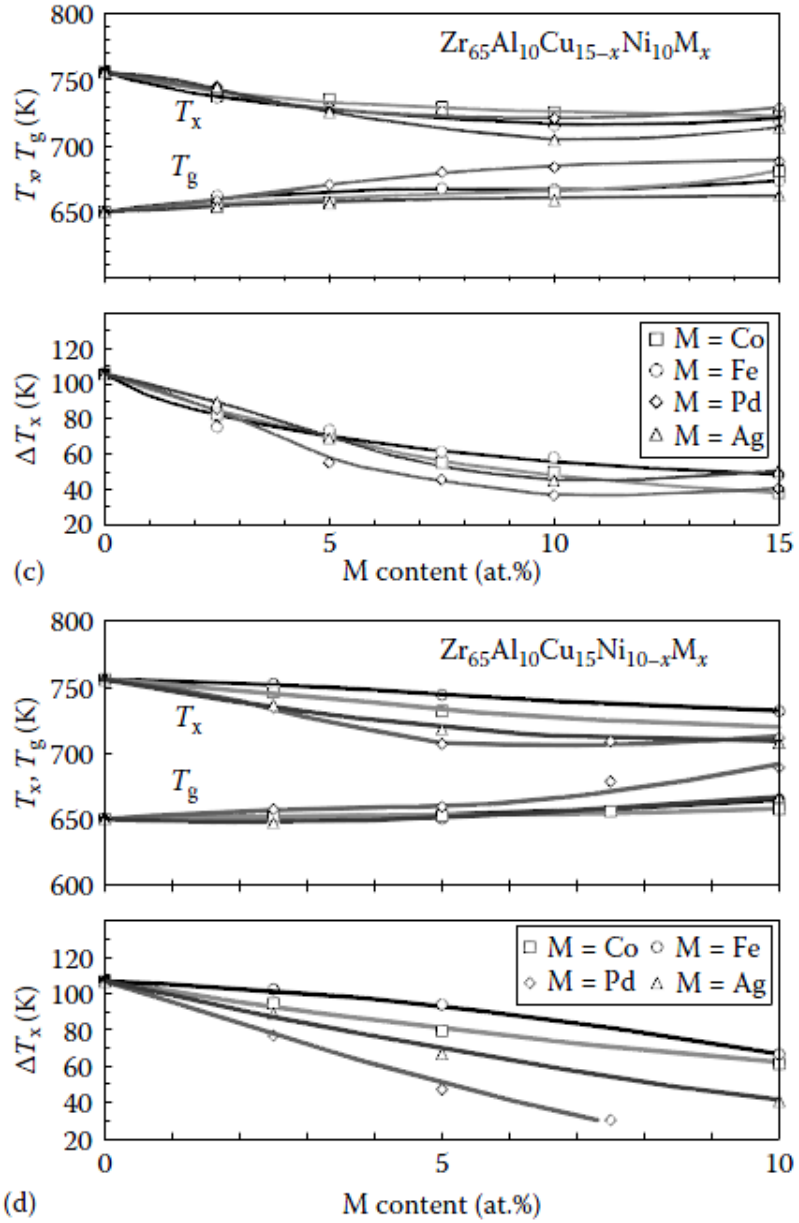

FIGURE 5.10 (continued)
(c) $Zr_{65}Al_{10}Cu_{15-x}Ni_{10}M_x$ (where M = Fe, Co, Pd, and Ag), and (d) $Zr_{65}Al_{10}Cu_{15}Ni_{10-x}M_x$ (where M = Fe, Co, Pd, and Ag). The T_g and T_x values were measured at a heating rate of 0.67 K s^{-1} (40 K min^{-1}). (Reprinted from Inoue, A. et al., *Mater. Trans., JIM*, 36, 1420, 1995. With permission.)